IL NUOVO CIMENTO Vol. 36 C, N. 2 Marzo-Aprile 2013
DOI 10.1393/ncc/i2013-11504-8

Colloquia: Nanoforum 2012

Optimization of thermochromic VO_2-based structures with tunable thermal emissivity

R. Li Voti(*), M. C. Larciprete, G. L. Leahu, M. Bertolotti and C. Sibilia

Dipartimento di Scienze di Base ed Applicate per l'Ingegneria, Sapienza Università di Roma Via A. Scarpa 16, 00161 Roma, Italy

ricevuto il 7 Marzo 2013

Summary. — In this paper we design and simulate VO_2/metal multilayers to obtain a large tunability of the thermal emissivity of IR filters in the typical MWIR window of many infrared cameras. The multilayer structure is optimized to realise a low-emissivity filter at high temperatures useful for military purposes. The values of tunability found for VO_2/metal multilayers are larger than the value for a single thick layer of VO_2. Innovative SiO_2/VO_2 synthetic opals are also investigated to enhance the optical tunability by combining the properties of a 3D periodic structure and the specific optical properties of vanadium dioxide.

PACS 78.20.Ci – Optical constants (including refractive index, complex dielectric constant, absorption, reflection and transmission coefficients, emissivity).
PACS 78.20.nb – Photothermal effects.
PACS 81.07.-b – Nanoscale materials and structures: fabrication and characterization.
PACS 42.70.Km – Infrared optical materials.

1. – Introduction

The term *infrared signature* generically describes how objects appear to infrared sensors. In most cases, infrared (IR) emissions from vehicles are used to detect, track, and lock-on to targets. The infrared signature of a given object depends on several factors, including the shape and size of the object, its temperature and its emissivity, as well as external conditions (illumination, background, to name some). One of the most challenging tasks regarding the IR vision is to reduce the infrared signature of objects. Although the IR spectrum extends from red light to microwave radiation, *i.e.* 0.77 to 1000 μm, there are only two wavelength ranges showing high IR transmittance in the atmosphere, *i.e.* 3–5 and 8–12 μm, known as the mid (MWIR) and long (LWIR) IR windows, respectively. Outside these windows, CO_2 and H_2O vapour give rise to both absorption and

(*) E-mail: roberto.livoti@uniroma1.it

scattering phenomena, producing strong attenuation of IR radiation. Thermochromic materials, changing their spectral properties as a function of the temperature, are extensively studied in the search for active control of thermal emission. These are for example niobium dioxide (NbO_2), vanadium sesquioxide (V_2O_3) and vanadium dioxide (VO_2). The most known and widely used is vanadium dioxide, VO_2, that is also the object of the present study [1]. Its crystalline lattice exhibits an abrupt semiconductor-to-metal phase transition at a temperature $T_C = 341\,K$ ($68\,^\circ C$), characterized by an increase of reflectivity as well as a decrease of emissivity in the IR range. On microscopic scales, the phase transition in VO_2 produces a physical change of its crystalline cell from monoclinic to tetragonal. VO_2 shows insulating behavior below T_C, whereas above this temperature it exploits a metallic nature, dramatically changing its optical, electrical and magnetic properties. In particular, the optical properties are sharply changed during the phase semiconductor-to-metal transition; thus the dispersion law of the complex refractive index $n + ik$ is strongly modified [2-4]. As a consequence, the phase transition, occurring during a very short temporal range of the order of few picoseconds, can be exploited for the realization of optical component switching from transparent (in the semiconductor state) to reflective (in the metallic state), as well as for efficient thermal switches [5, 6].

In general, the performance of either optical and thermal switches can be quantified and estimated through the so-called *dynamic range*, which is the difference between the largest and smallest possible values of a changeable quantity. Within the present work we define this figure of merit as the difference between the emissivity values, averaged in the IR range 3–5 μm and calculated for two different regimes, *i.e.* below and above T_C. Given this assumption, the *sign* of the dynamic range completely changes the filter behavior and thus determines the type of application. A thermochromic filter displaying positive dynamic range, *i.e.* an IR emissivity *decreasing* with increasing temperature, is suitable for IR signature reduction as well as for smart windows for thermal control [7]. On the other hand, a *negative* dynamic range is required for space applications and emissivity control of spacecraft [8]. Recent experimental and theoretical works have shown that the thermal emissivity variation with temperature (and the dynamic range) of VO_2 thin films is strongly influenced by the substrate used for the deposition [9, 10]. In what follows we consider simulations of the optical response of VO_2 thin films first deposited on different substrates (sect. **2**), and then in multilayer structures (sect. **3**), below and above the T_C. We discuss the effect that different substrates as well as VO_2 layer thicknesses have on the sign of the dynamic range. Finally, we introduce some metallo-dielectric multilayer structures, composed of alternating copper or silver and VO_2 layers, where the layer thickness is systematically varied in order to further increase and optimize the dynamic range.

2. – Thermal emissivity and infrared signature for VO_2 thin film

A study for the design and optimization of the VO_2 films may start from the calculation of the emissivity of VO_2 thin films on several different substrates with varying film thickness. As well known from Kirchhoff's law, the directional spectral emittance is equal to the directional spectral absorptance so that $\varepsilon = 1 - R - T$, where R and T, respectively, are the reflectance and transmittance of the structure. To compare the different structures one fundamental quality factor to be introduced is the *tunability of emissivity* defined as the difference of the emissivity of the cold film minus the emissivity of the hot film. This quantity is usually averaged over the narrow window of the particular infrared

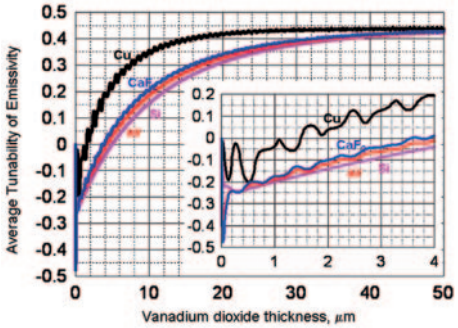

Fig. 1. – Average tunability of emissivity *vs.* the vanadium dioxide thickness for different substrates: copper (black line), silicon (pink line), calcium fluoride (blue line), none (red line). Inset: magnification of the small vanadium dioxide thickness range.

camera $[\lambda_{\min}, \lambda_{\max}]$ (in our example the MWIR window 3–5 μm) as follows [11,12]:

$$\Delta\varepsilon_{\mathrm{av}} = \frac{\int_{\lambda_{\min}}^{\lambda_{\max}} \Delta\varepsilon \mathrm{d}\lambda}{\lambda_{\max} - \lambda_{\min}} = \frac{\int_{\lambda_{\min}}^{\lambda_{\max}} (\varepsilon_{\mathrm{c}} - \varepsilon_{\mathrm{h}})\, \mathrm{d}\lambda}{\lambda_{\max} - \lambda_{\min}}, \tag{1}$$

where ε_{c}, ε_{h} correspond, respectively, to the emissivity of the filter when *cold* or *hot* with respect to the transition temperature. Figure 1 shows the average tunability of the emissivity $\Delta\varepsilon_{\mathrm{av}}$ as a function of the vanadium dioxide thickness. The curves refer to different substrates with optical properties taken from the literature: infrared transparent substrates (CaF_2: blue curve [13]. Si: pink curve [14]), infrared opaque or metallic substrate (copper: black curve [14,15]), and as a reference, a hypothetical free standing VO_2 film in air (red curve). The emissivity is here calculated as $\varepsilon = 1 - R - T$ for normal incidence by using transfer matrix method. In the figure the inset shows the behaviour at small VO_2 thickness (μm). The average tunability of emissivity might change sign on varying the vanadium dioxide thickness $d_{\mathrm{VO_2}}$. For example in the case of the VO_2/CaF_2 system (blue curve), the average tunability reaches a minimum value of about $\Delta\varepsilon_{\mathrm{av}} = -0.4$ for $d_{\mathrm{VO_2}} = 20\,\mathrm{nm}$ (thin layer), while for thick layers it changes sign giving $\Delta\varepsilon_{\mathrm{av}} > +0.3$ for $d_{\mathrm{VO_2}} = 20\,\mu\mathrm{m}$. This behaviour is confirmed from the simulated emissivity spectra shown in fig. 2. The emissivity of the sample with the thin VO_2 layer

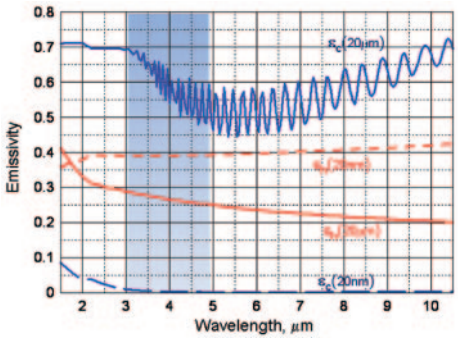

Fig. 2. – *Cold* and *hot* emissivity spectra of VO_2/CaF_2 for both thin and thick vanadium dioxide thicknesses. Cold 20 μm layer (blue solid line); hot 20 μm layer (red solid line); cold 20 nm layer (blue dotted line); cold 20 nm layer (red dotted line).

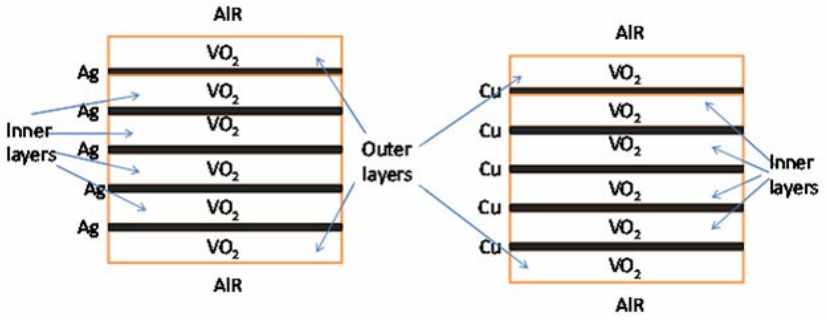

Fig. 3. – Sketch of the VO_2/Ag and VO_2/Cu multilayers structures. The number of layers is here for example $N = 11$.

(20 nm) increases with temperature (see dotted lines: blue for ε_c, red for ε_h), while the opposite happens for the sample with the thick VO_2 layer (20 μm) (see solid lines: blue for ε_c, red for ε_h). In this last case interference fringes also appear in both MWIR and LWIR (blue solid line). Their spacing is of the order of the wavelength, and the vanadium dioxide is in the semiconductor state.

In order to design an IR tunable filter, one must be able to reduce the infrared signature of hot objects; the requirement is to work with a structure with a large and positive tunability $\Delta\varepsilon_{av} > 0$. This is achieved by increasing the film thickness (see fig. 1), and also by using metallic absorbing substrates able to enhance the whole cold emissivity ε_c when vanadium dioxide is in the semiconducting state. The black curve in fig. 1, corresponding to a copper substrate, shows an enhancement of the tunability up to the limiting value of $\Delta\varepsilon_{av} = +0.45$. Similar behaviour is seen when using other metallic substrates. We may now ask if it is possible to achieve a further enhancement of the tunability by using a more complex structure which uses vanadium dioxide and metal layers.

3. – Signature reduction with an optimized VO_2/Metal multilayer

Here we study how to enhance the tunability of a single VO_2 film by designing an optimized VO_2/Metal multilayer structure acting as a *tunable transparent metal*. Transparent metals basically are 1D photonic band gap (PBG) multilayers which exhibit pass-band properties in the optical range. This unusual and rare property of transparency for metals is achieved by growing an adequate sequence of metal thin layers (≈ 10 nm) and transparent dielectric thick layers. Thanks to the tunnelling phenomena in the metal layers [16-18] and the interference effects in the dielectric layers [19,20], these structures are able to enhance the transmittance at some wavelengths. After some preliminary tests we have chosen to optimise a structure of fig. 3 which satisfies the following requirements [16,21]:

a) It is made up of an odd number N of layers. A number of $(N+1)/2$ VO_2 layers are alternated with a number of $(N-1)/2$ metallic layers.

b) The two outer vanadium dioxide layers have the same thickness $d_{\mathrm{ext}VO_2}$.

c) The inner vanadium dioxide layers have the same thickness $d_{\mathrm{int}VO_2}$.

d) Each metal layer (Cu or Ag) is 10 nm thick so to guarantee optical tunnelling.

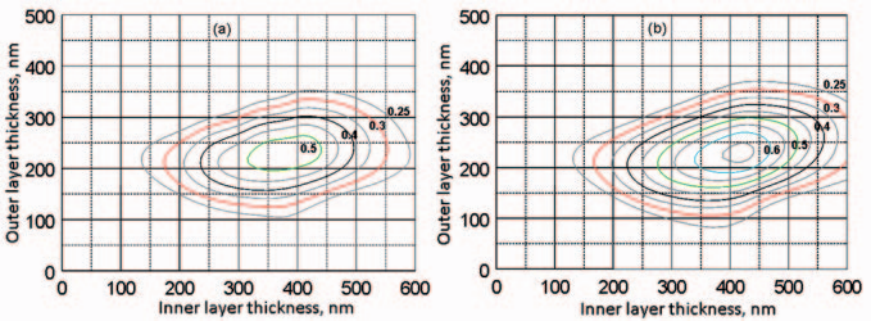

Fig. 4. – Contour plot of the average tunability of emissivity of VO_2/Cu multilayer as a function of the inner VO_2 layer thickness $d_{\mathrm{int}VO_2}$ and outer VO_2 layer thickness $d_{\mathrm{ext}VO_2}$ as introduced in fig. 3: (a) multilayered structure with $N = 9$ made of a total thickness of 40 nm of copper; (b) multilayered structure with $N = 21$ made of a total thickness of 100 nm of copper.

Although this structure does not maximize the number of degrees of freedom (*i.e.* thicknesses of the different layers), it is sufficiently flexible. An example of an optimization is reported for a VO_2/Cu structure made of $N = 9$ layers. The 4 layers of Cu are 10 nm thick. Simulations were made by changing the vanadium dioxide thicknesses of both the inner layers of thickness $d_{\mathrm{int}VO_2}$ and outer layers of thickness $d_{\mathrm{ext}VO_2}$ in the range 0–500 nm. The tunability of the emissivity for each layer pair $[d_{\mathrm{int}VO_2}, d_{\mathrm{ext}VO_2}]$ is shown using a contour plot in fig. 4a. The maximum of $\Delta\varepsilon_{\mathrm{av}} + 0.53$ is reached when 370 nm and $d_{\mathrm{ext}VO_2} = 230$ nm. Some remarks immediately follow.

a) The value $\Delta\varepsilon_{\mathrm{av}} + 0.53$ is larger than the asymptotic limit of +0.45 of fig. 1 obtained with a single thick layer of VO_2. This justifies the use of multilayered structures with thinner layers of VO_2 and metal. Note that the total amount of vanadium dioxide is less than 1.5 μm.

b) From the contours one may see that the choice of the optimal thicknesses $d_{\mathrm{int}VO_2}$ and $d_{\mathrm{ext}VO_2}$ is not critical and allows relatively large tolerances (20 nm).

b) Since a quarter wavelength layer of thickness $\lambda_0/4n \approx 300$ nm for *cold* vanadium dioxide ($< 68\,^{\circ}$C) is appropriate at the central wavelength $\lambda = 4\,\mu$m of the MWIR window, it appears that the optimized value $d_{\mathrm{int}VO_2} = 370$ nm follows the rules of quarter wavelength stacks normally used in antireflection structures. This implies that the optimization procedure converges towards structures with minimum reflection (at $T < 68\,^{\circ}$C) so to maximize the absorbance (*i.e.* emissivity) in the metal layers. This is clear in fig. 5 and 6. One can see that the quantity $\Delta\varepsilon_{\mathrm{av}}$ is also maximized.

The second example in fig. 4b shows the optimization for the same VO_2/Cu structure but with a very large number of layers ($N = 21$) in order to check if any asymptotic limit for the obtainable value of $\Delta\varepsilon_{\mathrm{av}}$ exists. The maximum of the average emissivity is now $\Delta\varepsilon_{\mathrm{av}} + 0.67$ for $d_{\mathrm{int}VO_2} = 420$ nm and $d_{\mathrm{ext}VO_2} = 230$ nm. As N increases there is an increase of $\Delta\varepsilon_{\mathrm{av}}$ and an adjustment of $d_{\mathrm{int}VO_2}$ which finally stabilizes to 420 nm.

The emissivity spectra of the VO_2/Cu optimized structures are shown in fig. 5a. As the number of layers increases (the arrow shows the sequence $N = 9, 11, 13, 15, 17$) the *cold* emissivity spectra ε_{c} also increases, tending to 1 (maximum emissivity) in the MWIR

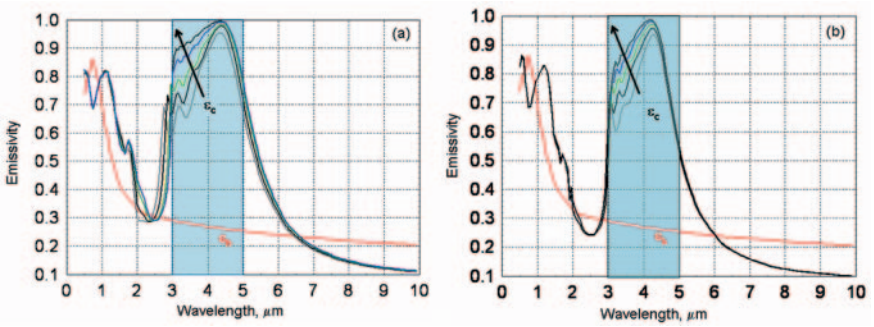

Fig. 5. – *Cold* and *hot* emissivity spectra for VO_2/Metal optimized multilayers. (a) Emissivity *vs.* wavelength for VO_2/Cu optimized multilayers. Red curve: *hot* emissivity ε_h at temperature $T > 68\,^\circ$C. Other colors: *cold* emissivity ε_c for multilayers with an increasing number of layers $N = 9, 11, 13, 15, 17$. (b) Emissivity *vs.* wavelength for VO_2/Ag optimized multilayers. Red curve: *hot* emissivity ε_h at temperature $T > 68\,^\circ$C. Other colors: *cold* emissivity ε_c for multilayers with an increasing number of layers $N = 9, 11, 13, 15, 17$.

window, whereas the *hot* emissivity spectra ε_h is practically unchanged because the IR emission comes entirely from the surface VO_2 layer that becomes a thick metallic layer for $T > 68\,^\circ$C. Figure 5b is the same as fig. 5a with silver substituting copper.

The reasons for the large *cold* emissivity ε_c in the MWIR window are clearly put into evidence in fig. 6 where both the reflectance (6a) and transmittance (6b) spectra are shown for the same VO_2/Cu optimized multilayers discussed in fig. 5a. As expected fig. 6a shows that for $T < 68\,^\circ$C these multilayers behave as antireflection nanostructures in the MWIR window; the reflectance curves R_c tend to 0 (thus maximizing $\varepsilon = 1 - R - T$) with slow or imperceptible improvement as N increases. On the other hand, fig. 6b shows that the *cold* transmittance T_c decreases with the number of layers. Since the

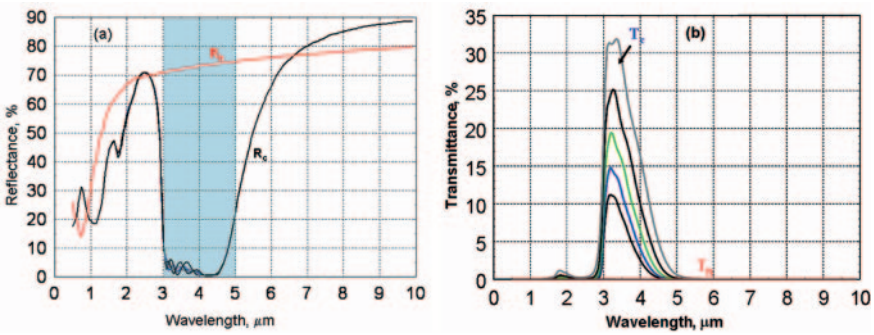

Fig. 6. – *Cold* and *hot* reflectance and transmittance spectra for VO_2/Cu optimized multilayers: (a) Optical reflectance *vs.* wavelength for VO_2/Cu optimized multilayers. Red curve: *hot* reflectance R_h at temperature $T > 68\,^\circ$C. Other colors: *cold* reflectance R_c for multilayers with an increasing number of layers $N = 9, 11, 13, 15, 17$. The curves are here undistinguishable. (b) Optical transmittance *vs.* wavelength for VO_2/Ag optimized multilayers. Red curve: *hot* transmittance T_h at temperature $> 68\,^\circ$C. Other colors: *cold* transmittance T_c for multilayers with an increasing number of layers $N = 9, 11, 13, 15, 17$.

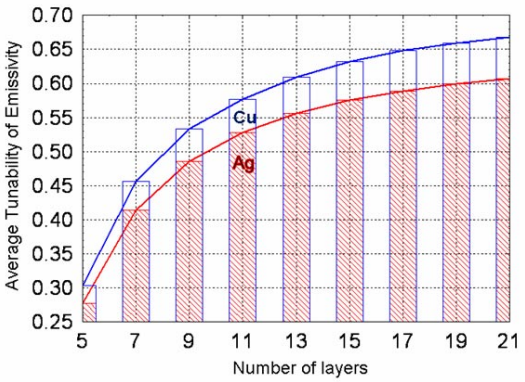

Fig. 7. – Maximum tunability of emissivity obtained with optimized multilayers VO_2/Ag based, and VO_2/Cu based as a function of the number of layers N. Each metal layer is 10 nm thick.

optimization procedure tends to maximize $\varepsilon_c = 1 - R_c - T_c$, this is obtained by simply increasing N (the arrow shows the sequence $N = 9, 11, 13, 15, 17$), so to increase the total amount of copper that can absorb light and consequently affect the emissivity. The emissivity spectra for VO_2/Ag-based structures are shown in fig. 5b; the arrow shows the sequence $N = 9, 11, 13, 15, 17$. In this case the structures are optimized asymptotically with $d_{\mathrm{int}VO_2} = 430\,\mathrm{nm}$ and $d_{\mathrm{ext}VO_2} = 240\,\mathrm{nm}$, but are less efficient than the VO_2/Cu-based ones when considering the value of $\Delta\varepsilon_{\mathrm{av}}$. The reason can be understood from a comparison between figs. 5a and 5b. The emissivity spectra for cold VO_2/Ag is narrow with respect to cold VO_2/Cu, and does not fit completely the MWIR window. These slight differences can quantitatively be shown in the average tunability of the emissivity as a function of N for the optimized VO_2/Ag- and VO_2/Cu-based multilayers as reported in fig. 7. Whatever the number of layers N, copper shows better results [11, 12].

4. – Optical tunability of 3D-VO_2 structures

Further enhancement of the tunability can be in principle obtained by using a 3D-VO_2 based photonic bandgap [22-24]. This nanostructure, so called *synthetic opal*, is the simplest method of synthesis of photonic crystals for visible light. The face-centered-cubic lattice is made up of close-packed submicron spheres (100 nm–600 nm) of amorphous silica. A sublattice of interconnected pores occupies the space between the spheres. The pores are filled in our case with VO_2 to create a 3D photonic crystal nanostructure which combines the properties of a 3D periodic opal structure and the specific optical and electrical properties of vanadium dioxide. In this way one may manipulate the fundamental properties of photonic crystals, and in particular the internal light propagation, absorption, scattering as well as emission. Another useful parameter in the design of these nanostructures is the filling factor that is the percentage of infiltration of vanadium dioxide inside the interconnected pores that may range from 40% to 60%. As example we report the experimental results on SiO_2/VO_2 opal samples produced by IOFFE Institute of S. Petersburg with different diameter of the SiO_2-spheres, and different filling factor of VO_2. The main properties for these samples are reported in table I [22-25].

To study the optical and photonic band gap properties of the samples, the specular reflection spectra from the (111) lattice planes of the opal-VO_2 composites has been measured by the IOFFE Institute of S. Petersburg. The Bragg reflection peaks measured

TABLE I. – *Properties of the samples made.*

Name	Diameter of SiO_2 beads nm	Filling % vol.	Thermal diffusivity m^2/s	Absorption depth @514 nm
K702	310	65 ± 5	-	-
K703	245	50 ± 5	5.4×10^{-7}	3.3 μm
K704	270	60 ± 5	5.4×10^{-7}	2.3 μm
K706	320	60 ± 5	5.6×10^{-7}	4.0 μm
K709	245	40 ± 5	5.3×10^{-7}	2.3 μm

at near normal light incidence (not shown here) occur at the proper wavelengths related to the size of the silica spheres and to the filling factor of the vanadium dioxide. In addition when the samples are heated, vanadium dioxide turns from semiconductor to metal and the Bragg peaks shift towards the short-wavelengths (blue shift). A simple detection of the tunability can be performed also by photothermal deflection spectroscopy (PDS) [26, 27]. In this experiment a Xe pump lamp is used as excitation light. The light passes through a monochromator in the range 250–1200 nm, and chopped at a low frequency (36 Hz). The light is eventually focused onto the sample and selectively absorbed so to produce an ac temperature rise. The He-Ne probe laser beam skims the sample surface, is deflected by the induced temperature gradient, and is eventually detected by a position sensor which measures the deflection angle. This signal is proportional to the ac temperature profile which increases with the sample absorption property. In synthesis the PDS spectrum represents the sample absorption spectrum. All the opals have been investigated by PDS in open air, but in order to increase the signal to noise ratio of 500 times, the samples have been also inserted in a cell filled with CCl_4 [25]. In fig. 8 the PDS spectrum for the samples K706 is reported for two temperatures below (20 °C) and above (85 °C) the transition temperature. The PDS spectra reveal a minimum of absorptance at around 800 nm in correspondence with the maximum of reflectance (Bragg peaks). As expected the peaks are subjected to a blue shift with temperature due to the semiconductor-to-metal transition of vanadium dioxide.

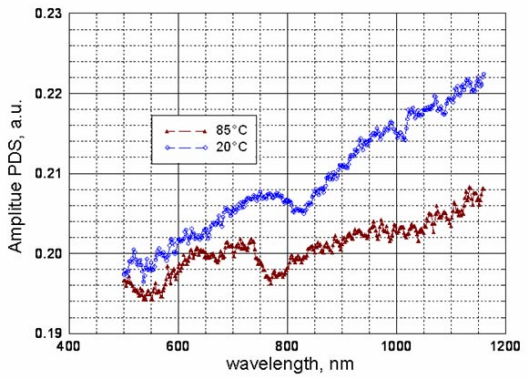

Fig. 8. – Photothermal deflection spectra for K706; blue: at 20 °C (below T_c), and brown: at 85 °C (above T_c).

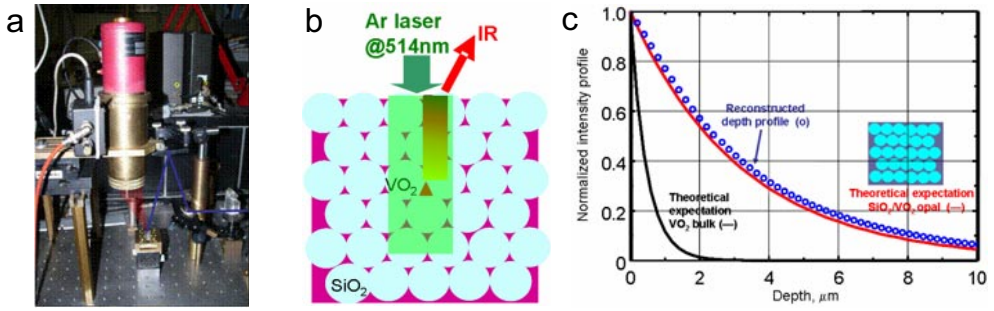

Fig. 9. – (a) Experimental radiometry setup, (b) internal heat source, (c) heat source depth profile by SVD *vs.* light intensity profile in a SiO_2/VO_2 synthetic opal.

More details on the light absorption in these nanostructures can be given by photothermal radiometry which has been recently acknowledged as useful indirect technique to visualize the light propagation in SiO_2/VO_2 opal structures according to the well known theory of depth profiling [28-32]. In the experiment the Ar pump laser beam is modulated by an acousto-optical modulator at a frequency ranging from 1 Hz to 100 kHz, and focused onto the opal structures (see fig. 9). The light is partially absorbed in the whole structure by the VO_2 crystallites regularly distributed in all the pores. Assuming that the heat is generated proportionally to the light intensity flowing in the structure, one may visualize the internal light propagation by performing the heat depth profile reconstruction from the photothermal radiometric data [32-36]. All the reconstructed profiles, obtained by using singular value decomposition, exhibit a quasi-exponential behaviour. In fig. 9 we report the heat source profile on a SiO_2/VO_2 synthetic opal (○). In the figure we also show the numerical simulations for the light intensity profile inside the opal (red continuous line) and inside a compact VO_2 film (black continuous line) that is obviously much more absorbed. The excellent agreement between SVD reconstruction and the numerical simulations show how this technique may be applied for nondestructive visualization of light intensity depth profile in these nanostructures. The absorption depth calculated as the penetration depth at which the light intensity is attenuated to 1/e is reported in table I for all the synthetic opals. The effective thermal diffusivity of the whole nanostructure is finally measured by photothermal deflection technique [36-40]. The thermal diffusivity values reported in table I put into evidence the role of the thermal boundary resistance among spheres [36].

5. – Conclusions

The results presented show the possibility of affecting the emissivity properties of VO_2 layers with temperature by playing with a number of different parameters, *i.e.* the layer thickness, the substrate material and the use of multilayer structures. The temporal response of the thermal transition is affected by all these parameters, and should be investigated in future experiments. New 3D geometries given by SiO_2/VO_2 synthetic opals, are also investigated to enhance the optical tunability by combining the properties of a 3D periodic structure and the specific optical and electrical properties of vanadium dioxide. For the characterization of these 3D nanostructures we demonstrate that photothermal deflection and radiometry may play a fundamental role.

* * *

This work has been performed in the framework of the contract "*FISEDA*" granted by Italian Ministry of Defence. The authors are grateful to the group of V. Golubev at IOFFE Institute of S. Petersburg for providing samples.

REFERENCES

[1] Qazilbash M. M., Brehm M., Chae B.-G., Ho P.-C., Andreev G. O., Kim B.-J., Yun S. J., Balatsky A. V., Maple M. B., Keilmann F., Kim H.-T. and Basov D. N., *Science*, **318** (2007) 1750.
[2] Kakiuvhida H., Jin P., Nakao S. and Tazawa M., *Jpn. J. Appl. Phys.*, **46** (2007) L113.
[3] Guzman G., Beteille F., Morineau R. and Livage J., *J. Mater. Chem.*, **6** (1996) 505.
[4] Konovalova O., Sidorov A. and Shagonov I., *J. Opt. Technol.*, **66** (1999) 391.
[5] Pevtsov A. B., Kurdyukov D. A., Golubev V. G., Akimov A. V., Meluchev A. A., Sel'kin A. V., Kaplyanskii A. A., Yakovlev D. R. and Bayer M., *Phys. Rev. B*, **75** (2007) 153101.
[6] Golubev V. G., Davydov V. Y., Kartenko N. F., Kurdyukov D. A., Medvedev A. V., Pevtsov A. B., Scherbakov A. V. and Shadrin E. B., *Appl. Phys. Lett.*, **79** (2001) 2127.
[7] Guinneton F., Sauques L., Valmatette J.-C., Cros F., and Gavarr J.-R., *Thin Solid Films*, **446** (2004) 287.
[8] Benkahoul M., Chaker M., Margot J., Haddad E., Kruzelecky R., Wong B., Jamroz W. and Poinas P., *Solar Energy Mater. Solar Cells*, **95** (2011) 3504.
[9] Choi H. S., Ahn J. S., Jung J. H., Noh T. W. and Kim D. H., *Phys. Rev. B*, **54** (1996) 4621.
[10] Dillon R., Le K. and Ianno N., *Thin Solid Films*, **398-399** (2001) 10.
[11] Li Voti R., Larciprete M. C., Leahu G., Sibilia C. and Bertolotti M., *J. Nanophoton.*, **6** (2012) 061601.
[12] Li Voti R., Larciprete M. C., Leahu G., Sibilia C. and Bertolotti M., *J. Appl. Phys.*, **112** (2012) 034305.
[13] Malitson I., *Appl. Optics*, **2** (1963) 1103.
[14] Palik E., *Handbook of optical constants of solids* (Academic Press, Inc. New York) 1985.
[15] Foiles C., *Optical properties of pure metals and binary alloys*, in *Landolt and Bornstein, Group III: Condensed Matter*, Vol. **15b**: *Electrical Resistivity, Thermoelectrical Power and Optical Properties*, edited by Hellwege K.-H. and Olsen J. (Springer-Verlag) 1985.
[16] Sarto M. S., Li Voti R., Sarto F. and Larciprete M. C., *IEEE Trans. Electromagn. Compat.*, **47** (2005) 602.
[17] Larciprete M. C., Sibilia C., Paoloni S., Bertolotti M., Sarto F. and Scalora M., *J. Appl. Phys.*, **93** (2003) 5013.
[18] Scalora M., Bloemer M., Manka A., Pethel S., Dowling J. and Bowden C., *J. Appl. Phys.*, **83** (1998) 2377.
[19] Larciprete M. C., Sibilia C., Paoloni S., Leahu G., Li Voti R., Bertolotti M., Scalora M. and Panajotov K., *J. Appl. Phys.*, **92** (2002) 2251.
[20] Larciprete M. C., Sibilia C., Paoloni S., Leahu G., Li Voti R., Bertolotti M. and Panajotov K., *Rev. Sci. Instrum.*, **74** (2003) 860.
[21] Li Voti R., *Rom. Rep. Phys.*, **64** (2012) 446.
[22] Golubev V. G., Kurdyukov D. A., Pevtsov A. B., Sel'kin A. V., Shadrin E. B., Il'inskii A. V. and Boeyink R., *Semiconductors*, **36** (2002) 1043.
[23] Golubev V. G., Kosobukin V. A., Kurdyukov D. A., Medvedev A. V. and Pevtsov A. B., *Semiconductors*, **35** (2001) 680.
[24] Pevtsov A. B., Kurdyukov D. A., Golubev V. G., Akimov A. V., Meluchev A. A., Sel'kin A. V., Kaplyanskii A. A., Yakovlev D. R. and Bayer M., *Phys. Rev. B*, **75** (2007) 153101.

[25] Leahu G., Li Voti R., Sibilia C., Bertolotti M., Golubev V. and Kurdyukov D. A., *Optical Quantum Electron.*, **39** (2007) 305.
[26] Boccara A. C., Fournier D. and Badoz J., *Appl. Phys. Lett.*, **36** (1980) 130.
[27] Jackson W. B., Amer N. M., Boccara A. C. and Fournier D., *Appl. Optics*, **20** (1981) 1333.
[28] Power J. F., *Rev. Sci. Instrum.*, **73** (2002) 4057.
[29] Glorieux C., Li Voti R., Thoen J., Bertolotti M. and Sibilia C., *Inverse Problems*, **15** (1999) 1149.
[30] Glorieux C., Li Voti R., Thoen J., Bertolotti M. and Sibilia C., *J. Appl. Phys.*, **85** (1999) 7059.
[31] Tomoda, M. Li Voti R., Matsuda O. and Wright O. B., *Appl. Phys. Lett.*, **90** (2007) 041114.
[32] Li Voti R., Sibilia C. and Bertolotti M., *Int. J. Thermophys.*, **26** (2005) 1833.
[33] Li Voti R., Liakhou G. L., Paoloni S., Sibilia C. and Bertolotti M., *J. Optoelectron. Adv. Mater.*, **3** (2001) 779.
[34] Bertolotti M., Liakhou G. L., Li Voti R., Paoloni S. and Sibilia C., *J. Appl. Phys.*, **85** (1999) 3540.
[35] Bertolotti M., Liakhou G. L., Li Voti R., Paoloni S. and Sibilia C., *Int. J. Thermophys.*, **19** (1998) 603.
[36] Li Voti R., *Proceedings of 2007 9th International Conference on Transparent Optical Networks, ICTON 2007*, **2** (2007) 192.
[37] Bertolotti M., Liakhou G., Li Voti R., Paoloni S. and Sibilia C., *J. Appl. Phys.*, **83** (1998) 966.
[38] Bertolotti M., Liakhou G., Li Voti R., Peng Wang R., Sibilia C. and Yakovlev V. P., *J. Appl. Phys.*, **74** (1993) 7054.
[39] Bertolotti M., Liakhou G., Ricciardiello F. G., Li Voti R., Paoloni S., Sibilia C., Tampieri A. and Sparvieri N., *J. Therm. Anal.*, **47** (1996) 67.
[40] Bertolotti M., Ferrari A., Liakhou G. L., Li Voti R., Marras A., Ezquerra T. A. and Balta-Calleja F. J., *J. Appl. Phys.*, **78** (1995) 5706.